Journal of Manufacturing Engineering, June, 2017, Vol. 12, Issue. 2, pp 82-93

MULTIOBJECTIVE OPTIMIZATION OF ATMOSPHERIC PLASMA SPRAY PROCESS PARAMETERS TO DEPOSIT ALUMINA COATINGS BASED ON RESPONSE SURFACE METHODOLOGY

Thirumalaikumarasamy D[1], Shanmugam K[2], V. Balasubramanian V[3] and *Kamal Jayaraj R[4]

[1]Assistant Professor, [2]Associate Professor, [3]Professor, [4]Research scholar, Department of Manufacturing Engineering, Annamalai University, Tamilnadu, India. .

ABSTRACT

Like other manufacturing processes, plasma spraying also has a non-linear behavior due to contribution of many coating parameters. This characteristic makes finding optimal factor combination difficult. The principle issue confronted in the manufacture of alumina coatings by the atmospheric plasma spraying process is the selection of the optimum combination of input variables for achieving the required qualities of coating. This problem can be solved by the development of empirical relationships between the process parameters (input power, stand-off distance and powder feed rate) and the responses (porosity level and corrosion rate). This article highlights the use of response surface methodology by designing a three-factor five level central composite rotatable design matrix with full replication for planning, conduction, execution and development of empirical relationships. Further, response surface methodology (RSM) was used to find out the optimum process parameters to achieve desired quality of alumina coating deposits.

Key words: *Plasma spraying process, Optimization, Response surface methodology, Alumina coating.*

1. Introduction

In recent years the interest in magnesium alloys is increasing due to their good properties, such as low density, high strength to weight ratio, good castability, good electromagnetic shielding characteristics, high dimensional stability and suitability for recycling [1,2]. These alloys are very promising, particularly for aerospace and automotive applications, to reducing fuel consumption and associated emission is a main goal [3]. The major problems that affect these alloys are low poor corrosion resistance and wear resistance, primarily attributed to the high chemical activity of magnesium alloy and to unstable the imperfect natural oxide film on its surface [4,5]. Surface treatments such as conversion coating, anodizing, plating, vapour deposition, plasma electrolytic oxidation, polymer coatings are the most common ways to improve the corrosion resistance of these materials. Among these, atmospheric plasma spraying (APS) is a newly developed but very promising process that can enhance the corrosion and wear resistance by producing a relatively thick, dense and hard oxide coating on magnesium alloys.

Plasma spray coating process is an effective surface engineering technique for its good thermal protectiveness, high hardness, and its wear resistance.

The process envelops a wide range of industrial applications including manufacturing, paper industries, and so on [6]. Atmospheric plasma spraying (APS) is governed by a number of parameters in order to get desired products. The plasma spray coating process does not have any robust mathematical formulation or model, which can be used to predict its input–output relationships.

Thermal sprayed ceramic coatings, such as alumina, zirconia and cordierite, offer cost-effective alternative to modify the component surface properties and are used in a wide range of industrial applications, primarily for wear resistance, thermal barrier and corrosive environment [7]. During plasma spraying, the precursor powders are feed into plasma discharge, where the powders melt and form small droplets which are accelerated toward the substrate. The droplets impact on the matrix, spread out and solidify to build up lames or splats. The laminar microstructure is highly defective with weak interfaces and voids between splats as well as un-melted particles and cracks. The discrete weak interface structure is directly related with properties of the plasma coating [8]. When plasma sprayed coatings exposed in aggressive media, electrolyte could penetrate the coating through the

*Corresponding Author - E- mail: jayaraj_kamal@yahoo.co.in

permeable defects such as cracks, pores and grain boundaries. Since most coating materials are nobler than the substrate, once the electrolyte approaches the substrate, the galvanic pair would be formed between the two systems and leads to a preferential corrosion of the material [9]. Therefore, reduction of volume of porosity in the sprayed coatings plays a key role in improving the corrosion resistance of the coatings.

Lin et al. [10] combined response surface methodology (RSM) and Taguchi design of experiments to correlate empirical relationship between plasma spraying parameters and oxidant percent. They also attempted to validate their model with analysis of variances (ANOVA) and confirmatory experiments. In another attempt, Lin et al. [11] combined Taguchi DOE with RSM to model the hardness of plasma-sprayed surface. They used statistical ANOVA to determine contribution of process factors on hardness. Although, they reported the optimal solution regarding highest hardness and developed accurate empirical model, but they lacked to analyze effects of factors on hardness according to physical meaning of the process.

However, optimization of plasma spray process involving multiple factors and multiple responses has hardly been reported in the literature. Hence, this article deals with the application of RSM in developing empirical relationships relating important input variables, namely, the power (P), the stand-off distance (S), and the powder feed rate (F), to the porosity, and the corrosion rate of the APS-Al_2O_3 coatings. Further, this article illustrates how a number of overlapping response surfaces can be used to select the operating conditions necessary to achieve the desired specifications and for the optimization of the plasma spraying process. It should be emphasized that the range selected for parameters, the results, and the conclusions refer specifically to the torch, the chemical composition, and the morphology of the powder material used in this study. However, the illustrated approach and the methodology of the response surfaces are universal.

2. Experimental procedure

In the present study, commercially available alumina ceramic powder (AMPERIT 740.1) was identified as the coating material. Fig. 1(a and b) shows the morphology of the as received power under scanning electron microscope (SEM) with particle sizes in the range of −45 to +20 µm. As a result of its fused and crushed shape, it also showed a very good flowability during spraying. The chemical composition of the powder was confirmed by an electron dispersive spectrometer (EDS) analysis (Fig. 1(c)). The substrate

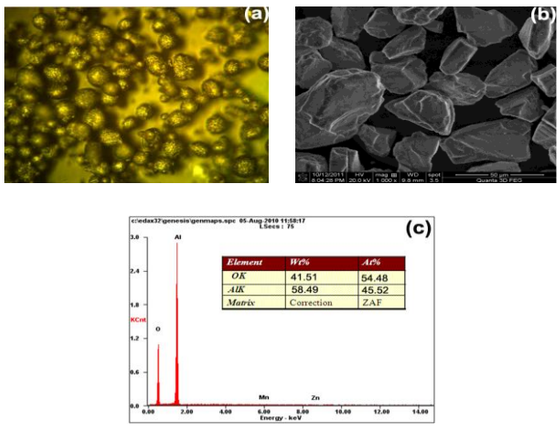

Fig. 1 (a&b) OM and SEM micrograph of alumina powder and (c) EDS analysis of Al_2O_3 powder.

selected for coating this material was commercial grade AZ31B magnesium alloy, which is mainly used for the aerospace, automobile, and railway industries. The nominal chemical composition (wt.%) of experimental alloy AZ31B Mg (as received) was; Al—3.0%, Mn—0.20%, Zn—1 %, and Mg—balance and it has the following mechanical properties: yield strength—171 MPa, ultimate tensile strength—215 MPa, elongation—14.7%, reduction in cross-sectional area—14.3%, and hardness at 0.05-kg load—69.3 Hv. Substrates with the dimension of 16 mm × 15 mm were grit-blasted on one side to clean and roughen the surface prior to deposition of the coating. Corundum, grit size of 320 ± 500 µm (Supplied by Metallizing Equipment Co. Jodhpur, India) was used to increase the surface roughness of the substrate. A surface roughness tester (Make: Mitutoyo, Japan; Model: Surftest 301) was used to measure the roughness and the average roughness of the substrate after grit blasting was found to be in the range of 5–10 µm. Commercial APS (Make: Ion Arc Technologies; India. Model: APSS-II) spraying system available at the Annamalai University, India, was used to deposit alumina coatings with a thickness of 240µm. The thickness of the coatings was measured by a digital micrometer (with an accuracy of 0.001 mm) for each and every run conditions. The APS spray process parameters employed along with the results obtained in terms of porosity and corrosion rate are shown in Fig. 2.

From the published literature [12-13] and our laboratory investigations [14], the predominant factors having significant influence on the performance of APS coatings were found to be power (P), spray distance (S)

and powder feed rate (F). Since these process variables have greater influence on coating characteristics and the resultant properties, it is necessary to determine the optimum levels of these variables with an objective to achieve minimum porosity and corrosion rate in the coatings.

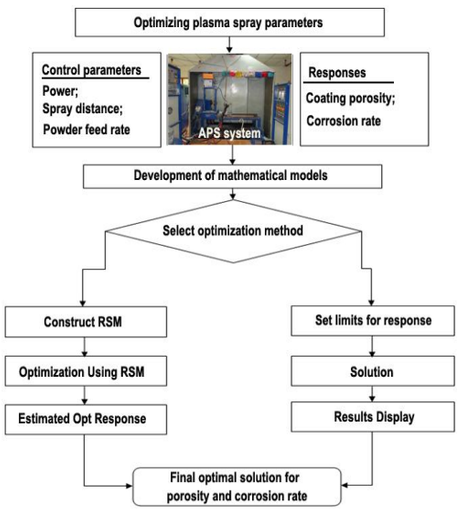

Fig. 2 Flow chart shows methodology adopted in this investigation.

A large number of experiments were conducted by atmospheric plasma spraying alumina powders on AZ31B substrate to determine the feasible working range of the above mentioned process variables by varying one of the parameters at a time and keeping others constant. The working range was arrived at taking into consideration the absence of coating defects such as poor adhesion to the substrate, unmelted powder particle in the coating, large porosity, cracks and lamellae solidified with columnar crystals (Table 1). Photographs of alumina coated specimens are shown in Fig. 3. As per the procedure laid out in ASTM B 276 standard (2010), the porosity measurement was carried out on the well-polished cross-sectional area of the coating, using an optical microscope (Make: Meiji; Japan, Model: MIL-7100) equipped with an image analyzing software (Metal Vison Version 6). In this study, the images captured under 1000× magnification by optical microscopy were chosen for porosity analysis as desired features like open pores and network of cracks were properly revealed. Initially, a 400 × 400 μm square area was selected on the polished cross-section of the coating and the image was analyzed as seen in Fig. 4(a–b). The same procedure was repeated at five random locations to find out the average percentage volume of porosity.

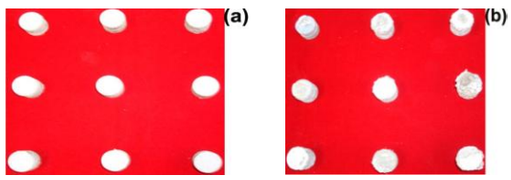

Fig. 3 Photographs of alumina coated specimens.

Immersion test was carried out to evaluate the corrosion behaviour of the alumina coated Mg alloys as per the ASTM G 31-72 standard 2002 [15]. The specimens were ground with 500#, 800#, 1200#, 1500# grit SiC paper washed with distilled water and dried by warm flowing air. The corrosion rates of the coated samples were estimated through the weight loss measurement. The original weight (WO) of the specimen were recorded and then immersed in the solution of 3.5% NaCl solution for 6 h. Finally, the corrosion products were removed by immersing the specimens for one minute in the solution prepared by using 50 g chromium trioxide (CrO3), 2.5 g silver nitrate (AgNO3) and 5 g barium nitrate (Ba(NO3)2) for 250 ml distilled water. The final weight (wt) of the specimen was measured and the net weight loss was calculated using the following equation:

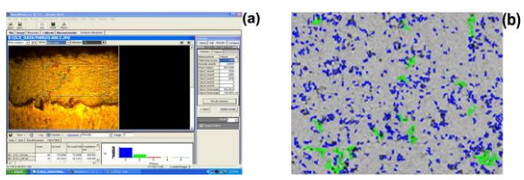

Fig. 4 Measure the porosity level using computer image analyzing software.

$$\text{Corrosion rate (CR)} = \frac{87.6 \times W}{A \times D \times T} \quad (1)$$

where W = weight loss in mg, A = surface area of the specimen in cm^2, D = density of the coated sample, T = corrosion time in h.

In this present study, RSM using central composite design was applied with full replication technique. Based on the experimental results, three predominant variables namely, power, spray distance and powder feed rate were selected. For recording the responses due to changes in these variables, every selected variable was operated at five different levels (−1.682, −1, 0, 1, 1.682) and the values of these

variables corresponding to these levels are shown in Table 2.

2.1 Coating Characterization

The SEM micrographs of the plasma-sprayed alumina coating are shown in Fig. 5(a). Spattering pattern appears on the surface, which indicates the occurrence of spraying molten drops during coating process. The alumina coatings consist of countless single spots from which a few circular pores are present on the coating surface, the non-uniform growing pattern of the coating and trapping of oxygen bubbles in the coating growth process may be responsible for the extensive porosity of the ceramic coating. The backscattered scanning electron micrographs of the cross-sections of the alumina coating revealed the very rough surface, interconnected pores randomly distributed within the layer and poor bonding at the substrate/coating interface (Fig. 5b). The XRD spectrum of the alumina coating is shown in Fig. 6. The coating mainly constituted of both α-Al_2O_3 [Joint Committee on Powder Diffraction Standards (JCPDS) card no. 46-1212] and β-Al_2O_3 (JCPDS card no. 10-0425).

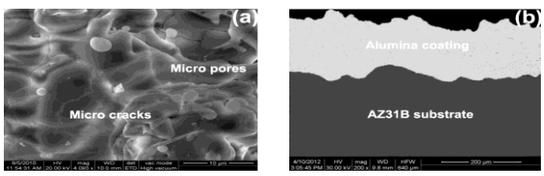

Fig. 5 SEM images of the alumina coating produced on AZ31 Mg alloy: (a) surface morphology and (b) cross-section morphology

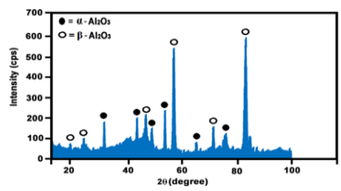

Fig. 6 XRD pattern of the as sprayed coating

3. Developing empirical relationships to predict coating porosity and corrosion rate

In order to determine the optimum levels of the process variables studied and their relationships, RSM concept was employed. RSM is a combination of mathematical and statistical techniques that are generally used for DOE, development of a mathematical model, identification of optimum combination of input parameters, and graphical expression of results for better understanding [16].

The relationship between the variables and the response after analysis was determined using the second order polynomial equation [17].

$$Y = \beta_o + \Sigma\beta_i x_i + \Sigma\beta_{ii} x_i^2 + \Sigma\beta_{ij} x_i x_j \quad (2)$$

where, Y is the predicted response, X_i, X_i^2, and X_j are variables in coded values; β_0 is the constant; β_i is the linear effect; β_{ii} is the squared effect and β_{ij} is the interaction effect. The analysis of results was performed with statistical and graphical analysis software (Design Expert, Version 8). The software was used for regression analysis of the data obtained and to estimate the coefficient of regression equation. Table 2 presents the feasible working limits of plasma spraying process parameters, and the other relevant parameters kept constant during plasma spraying are listed in Table 3. The 20 sets of coded conditions used to conduct the experiments are shown in Table 4.

The porosity and corrosion rate of the atmospheric plasma sprayed coatings are functions of power (P), spray distance (S), and powder feed rate (F), and it can be expressed as

$$\text{Responses} = f(P, S, F) \quad (3)$$

For the three factors, the selected polynomial can be expressed as

$$Y = b_0 + b_1(P) + b_2(S) + b_3(F) + b_{11}(P^2) + b_{22}(S^2) + b_{33}(F^2) + b_{12}(PS) + b_{13}(PF) + b_{23}(SF) \quad (4)$$

where, b_0 is the average of the responses and b_1, b_2, b_3, …, b_{44} are regression coefficients that depend on respective linear, interaction, and squared terms of factors. The final statistical model to estimate the responses are given below:

$$\text{Porosity level (vol.\%)} = 5.32 + 2.50(P) + 1.69(S) + 1.30(F) - 0.87(PS) + 0.88(PF) + 1.38(SF) + 1.54(P^2) + 2.42(S^2) + 1.72(F^2) \quad (5)$$

$$\text{Corrosion rate (mm/year)} = 5.22 - 1.84(P) + 1.54(S) + 0.34(F) + 0.71(PS) + 1.23(PF) + 1.35(SF) + 3.89(P^2) + 2.67(S^2) + 0.53(F^2) \quad (6)$$

3.1 Checking the Adequacy of the Model

In this investigation, analysis of variance (ANOVA) is used to check the adequacy of the developed empirical relationships [18]. ANOVA test

results of the responses, namely, the porosity level and corrosion rate are presented in Table 5 and 6, respectively. The adequacy of the model was tested using the ANOVA technique. In this study, the model F value and the associated probability values are checked to confirm the significance of the empirical relationships. Further, using the F-values, the predominant factors which have the major and minor effects on the responses could be assessed. From the F value assessment, it was found that the predominant factors which have direct influence on the responses as per hierarchy are power, spray distance and powder feed rate. The determination coefficient (R2) indicates the goodness of fit for the model. In all the cases, the value of the determination coefficient (R2 > 0.99) indicates that less than 1% of the total variations are not explained by the empirical relationships. The value of the adjusted determination coefficient is also high, which indicates the high significance of the empirical relationships. The predicted R2 values also show good agreement with the adjusted R2 values. Adequate precision compares the range of the predicted values at the design points with the average prediction error. At the same time, a relatively low value of the coefficient of variation indicates the improved precision and the reliability of the conducted experiments. The value of probability > F in Table 5 and 6 for the empirical relationships are less than 0.05, which indicates that the empirical relationships are significant. Lack of fit was not significant for all the developed empirical relationships as desired [19]. The normal probability plots for the responses are shown in Fig. 7. From the Fig., it could be inferred that the residuals fall on the straight line, which shows that the errors are distributed normally [20]. Collectively, these results indicate the excellent capability of the regression model. Further, each observed value matches its experimental value well, as shown in Fig. 8.

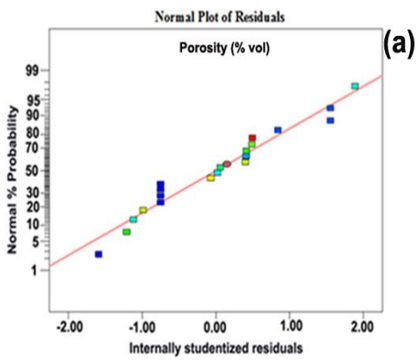

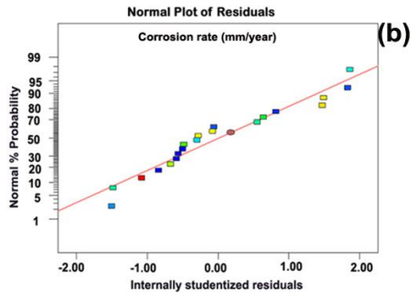

Fig. 7 Normal probability plots for the responses

4. Process Optimization

To investigate the influencing tendency of the process parameters on the responses, 3D graphs were plotted under certain processing conditions. The 3D response surface and 2D contour plots are the graphical representations of the regression equations used to determine the optimum values of the variables within the ranges considered [21]. Equation 5 (porosity level) was used to plot the Fig. 9(a)-(c) (surface plots) and 10(a)-(c) (contour plots). Equation 6 (corrosion rate) was used to plot the Fig. 9(d)-(f) (surface plots) and 10(d)-(f) (contour plots). From the Fig. 9 (a)-(c), it is proposed that the porosity level decreases, reaches a trough, and increases with the increase in the levels of considered process parameters. The valley (trough) of the response plot shows the minimum porosity level (the same trend was observed in the case of corrosion rate). These response contours can help in the prediction of the responses for any zone of the experimental domain.

The optimization part in Design-Expert software V8 searches for a combination of factor levels that simultaneously satisfy the requirements placed (i.e., optimization criteria) on each one of the responses and process factors (i.e., multiple-response optimization) [22]. Numerical and graphical optimization methods were used in this study by selecting the desired goals for each factor and response.

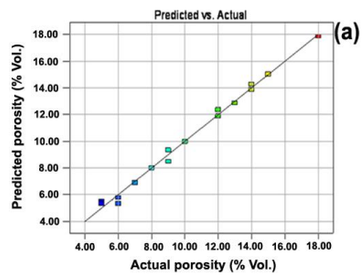

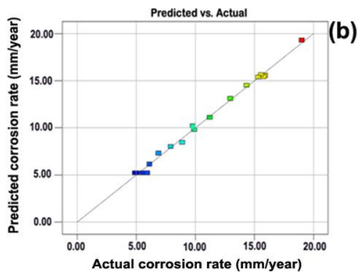

Fig. 8 Correlation plots for the responses

As mentioned before, the numerical optimization process involves combining the goals into an overall desirability function. The numerical optimization feature in the design expert package finds one point or more in the factors domain that would maximize this objective function. In a graphical optimization with multiple responses, the software defines regions where requirement simultaneously meet the proposed criteria. Also, superimposing or overlaying critical response contours can be defined on a contour plot. Then, a visual search for the best compromise becomes possible. In case of dealing with the many responses, it is recommended to run numerical optimization first; otherwise it is impossible to find out a feasible region. The graphical optimization displays the area of feasible response values in the factor space. Regions that do not fit the optimization criteria are shaded [23].

In the numerical optimization part, a criterion was adopted. The criterion is to minimize porosity volume and corrosion rate. In the case of graphical optimization for each response, the limits—lower and/or upper—have been chosen according to the numerical optimization results. The same criterion, which is proposed in the numerical optimization, was introduced in the graphical optimization. Contour plots play a very important role in the study of a response surface. The contour plots are illustrated in the Fig. 10(a)-(c) (porosity level) and Fig. 10(d)-(f) (corrosion rate). Each contour curve represents an infinite number of combinations of values of two test factors derived from the second-order quadratic equation within the considered range. The maximum predicted value is identified by the surface confined in the smallest ellipse or circle of the contour diagram. The circular contour plot indicates that the interactions between the corresponding factors are negligible, while the elliptical contour plot indicates that the interactions between the corresponding factors are significant. Furthermore, a contour plot is produced to display the region of the optimal factor settings visually. For second order response surfaces, such a plot can be more complex compared to the simple series of parallel lines that can occur with first-order empirical relationships. Once the stationary point is found, it is usually necessary to characterize the response surface in the immediate vicinity of the point. Characterization involves identifying whether the stationary point found is a minimum response or maximum response or a saddle point. To classify this, it is most straightforward to examine it through a contour plot [24]. By performing the numerical optimization, i.e., by solving Eqn 5 and 6, analyzing the profile of the response surfaces and their corresponding contour plots (Fig. 10 a-c, d-f), the response values are obtained. The above mentioned response values could be achieved using the following optimized parameter settings of power of 22.25 kW, spray distance of 11.52 cm and powder feed rate of 19.00 gpm. The above values (factor values and response values) were also verified using the graphical optimization. The graphical optimization result allows visual inspection to choose the optimum coating condition. The result of the graphical optimization are the overlay plots, this type of plots are extremely practical for quick technical use in the workshop to choose the values of the plasma spraying parameters that would achieve certain response value for this type of coatings. The shaded areas on the overlay plot are the regions that do not meet the proposed criteria [25]. The graphical optimization plot is displayed in Fig. 11.

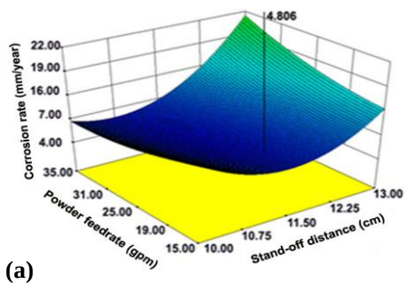

(a)

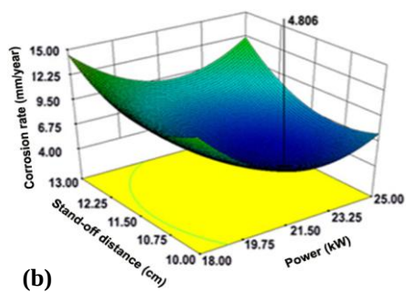

(b)

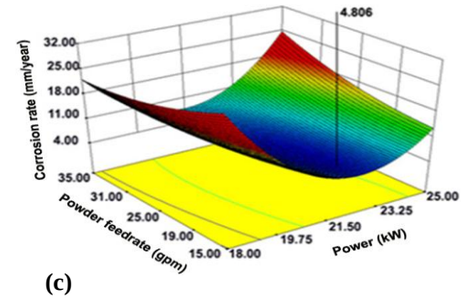

(c)

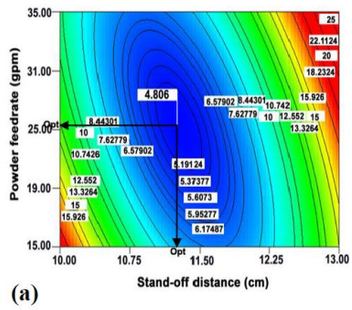

(a)

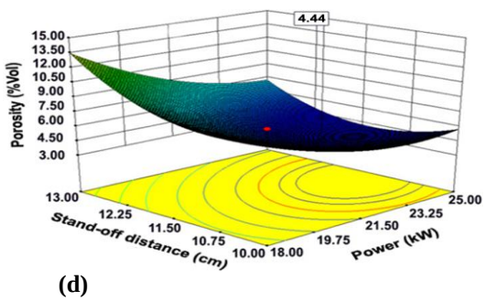

(d)

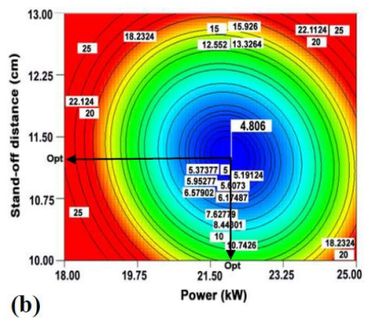

(b)

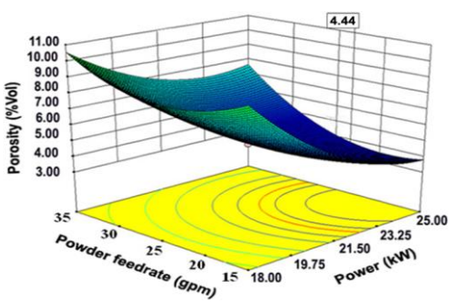

(e)

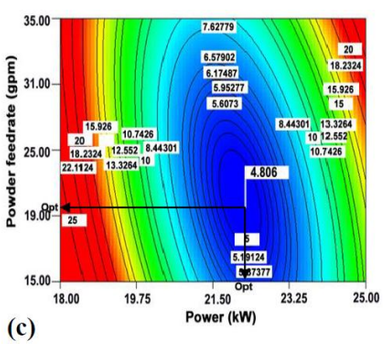

(c)

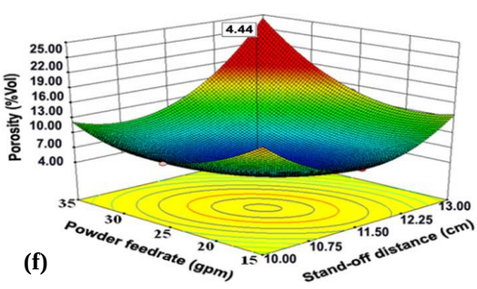

(f)

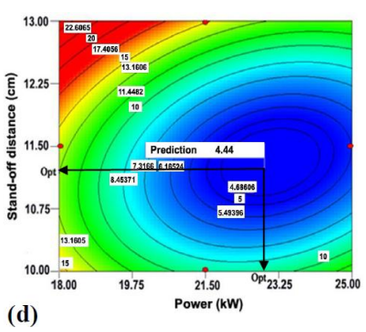

(d)

Fig. 9 Surface plots

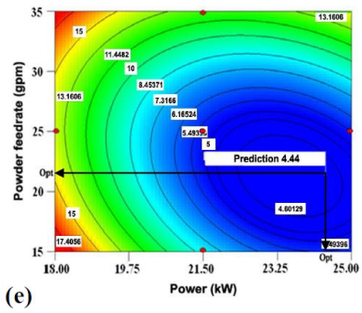

(e)

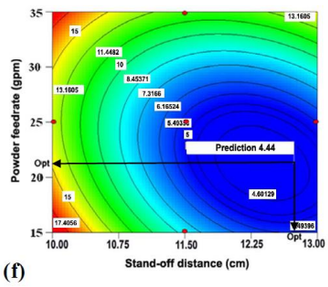

(f)

Fig. 10 (a)-(f) Contour plots

Table 1 Microstructure observation for fixing the working range of parameters

Sl no	*Parameters*	*Parameter Range*	*Microstructure*	*Name of the defect*
1	Power	<18 kW	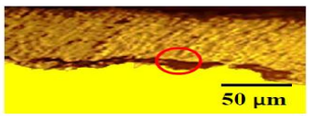	Coating delamination
2	Power	>18 kW	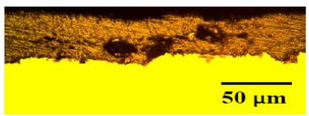	Poor deposition efficiency
3	Spray distance	<10cm	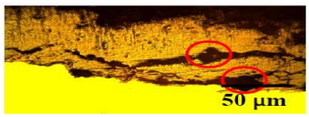	Peeling-off of the coating
4	Spray distance	>13cm		Poor coating adhesion

Table 2 Important APS process parameters and their levels

Factors	*Notations*	*Units*	*Levels*				
			-1.682	*-1*	*0*	*+1*	*1.682*
Power	*P*	kW	18	19.4	21.5	23.6	25
Stand-off distance	*S*	cm	10	10.6	11.5	12.4	13
Powder feed rate	*F*	gpm	15	19	25	31	35

Table 3 Other relevant parameters kept constant during plasma spraying

Parameters	**Alumina coating**
Primary gas (Argon) flow rate	38 lpm
Secondary gas (Nitrogen) flow rate	4 lpm

Table 4 Design matrix and Experimental Results

Expt Number	Coded values			Original value			Porosity level (vol. %)	Corrosion Rate (mm/year)
	P	S	F	P (kW)	S (cm)	F (gpm)		
1	-1	-1	-1	19.4	10.6	20	12	15.92
2	1	-1	-1	23.6	10.6	20	7	7.92
3	-1	1	-1	19.4	12.4	20	14	14.35
4	1	1	-1	23.6	12.4	20	6	9.92
5	-1	-1	1	19.4	10.6	30	10	11.23
6	1	-1	1	23.6	10.6	30	9	8.90
7	-1	1	1	19.4	12.4	30	18	15.80
8	1	1	1	23.6	12.4	30	13	15.56
9	-1.682	0	0	18	11.5	25	14	19.02
10	1.682	0	0	25	11.5	25	5	12.98
11	0	-1.68	0	21.5	10	25	9	9.80
12	0	1.682	0	21.5	13	25	15	15.34
13	0	0	-1.682	21.5	11.5	15	8	6.12
14	0	0	1.682	21.5	11.5	35	12	6.89
15	0	0	0	21.5	11.5	25	5	5.02
16	0	0	0	21.5	11.5	25	6	4.98
17	0	0	0	21.5	11.5	25	5	5.53
18	0	0	0	21.5	11.5	25	6	4.89
19	0	0	0	21.5	11.5	25	5	5.92
20	0	0	0	21.5	11.5	25	5	4.99

Table 6 ANOVA test results for corrosion rate

Source	*Sum of squares*	*df*	*Mean square*	*F value*	*p-value Prob > F*	
Model	404.847	9	44.983	249.2319	< 0.0001	**Significant**
P	46.35474	1	46.35474	256.8322	< 0.0001	
S	32.24242	1	32.24242	178.6417	< 0.0001	
F	1.623079	1	1.623079	8.992797	0.0134	
PS	4.013228	1	4.013228	22.23561	0.0008	
PF	12.15097	1	12.15097	67.32342	< 0.0001	
SF	14.56596	1	14.56596	80.70388	< 0.0001	
P^2	217.629	1	217.629	1205.791	< 0.0001	
S^2	103.0545	1	103.0545	570.9817	< 0.0001	
F^2	4.056546	1	4.056546	22.47561	0.0008	
Residual	1.804865	10	0.180487			
Lack of Fit	0.961151	5	0.19223	1.139189	0.4449	**Not significant**
Pure Error	0.843715	5	0.168743			
Cor Total	406.6519	19				
Std. Dev.	0.424837	**R-Squared**		0.995562		
Mean	10.05754	**Adj R-Squared**		0.991567		
C.V. %	4.224065	**Pred R-Squared**		0.978082		
PRESS	8.912924	**Adeq Precision**		46.90273		

df: degrees of freedom; CV: coefficient of variation; *F*: Fisher ratio; *p*: probability

The optical micrograph of the cross section of the coating produced under optimized processing condition is shown in Fig. 12. From Fig. 12, it could be inferred that the microstructure of the coatings is strongly dependent on processing conditions. When an adequately molten particle hits the substrate, the sudden deceleration causes a pressure build-up at the particle-substrate interface; the high pressure inside the particle forces the melted material to flow laterally or the ductile solid material to deform. The liquid spreads outward from the point of impact and forms a splat. The arresting of spreading results from the conversion of the particle kinetic energy into the work of viscous deformation and surface energy.

The process of splat formation depends on the velocity, size, molten state, chemistry, and angle of impact of the droplets on the surface. It is also subject to the surface topography of the substrate, its temperature, and

reactivity [26]. This process determines both microstructural and macroscopic characteristics of the coating. Optimum temperature of the particle corresponds to a decrease in the dynamic viscosity of the material, which together with optimum particle velocity, results in a higher degree of flattening. In addition, a higher degree of flattening corresponds to a decrease in splat thickness and a larger area of splat surface being in contact with the underlying material [27], which leads to a higher deposition efficiency, bond strength, microhardness, and low porosity. In the case of the coating produced under optimum spray conditions, owing to adequate in-flight temperature, most particles undergo melting, so that each splat covers more easily the surface topography onto which it flattens. The alumina coatings sprayed under the optimum condition can be used to produce coatings with the lowest porosity level and at relatively good corrosion protection.

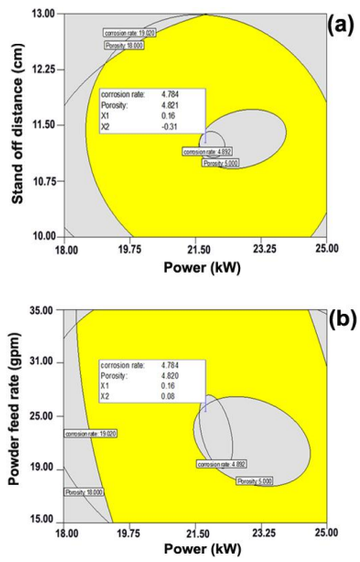

Fig. 11 Overlay plots

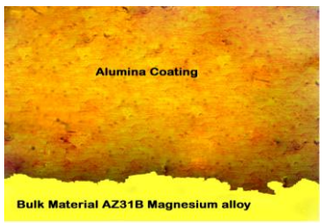

Fig. 12 Optical micrograph of the cross section of the coating deposited under optimized processing condition

5. Conclusions

The effects of APS parameters (power, spray distance and powder feed rate) on the porosity and corrosion rate were investigated for alumina coatings on magnesium alloy by adopting multiple objective optimization with RSM.

These results were used to develop empirical relationships to predict the optimum deposition conditions. From the F value assessment, it was found that power has the maximum influence on coating porosity and corrosion than that of other atmospheric plasma spray (APS) parameters.

Response graphs and contour plots were constructed incorporating the atmospheric plasma spray (APS) parameters to identify the minimum porosity and corrosion rate domains. It was found that the plasma

spray parameters such as with an input power of 22.25 kW, spray distance of 11.52 cm and powder feed rate of 19.00 gpm yielded minimum porosity (4.44 vol.%) and corrosion rate (4.806 mm/year) in coatings.

A regression equation has been developed by incorporating the responses such as porosity and corrosion rate of the plasma sprayed alumina coatings. This equation can be effectively used to predict plasma sprayed corrosion rate of alumina coating, if the coating porosity is known.

Input power was more sensitive than the other parameters such as stand-off distance and powder feed rate.

References

1. *Mordike B L and Ebert T (2001), "Magnesium properties—applications—potential", Materials Science and Engineering: A, Vol.302(1), 37–45.*

2. *Song G and Atrens A (2003), "Understanding magnesium corrosion — A framework for improved alloy performance", Advanced Engineering Materials, Vol.5(12), 837–858.*

3. *Nemcova A, Skeldon P, Thompson GE and Pacal B (2013), "Effect of fluoride on plasma electrolytic oxidation of AZ61 magnesium alloy", Surface and Coatings Technology, Vol.232(15), 827–838.*

4. *Liang J, Bala Srinivasan P, Blawert C, Stormer M and Dietzel W (2009), "Electrochemical corrosion behaviour of plasma electrolytic oxidation coatings on AM50 magnesium alloy formed in silicate and phosphate based electrolytes", Electrochimica Acta, Vol.54(4), 3842–3850.*

5. *Wang L, Chen L, Yan Z C, Wang HL and Peng J Z (2009), "Growth and corrosion characteristics of plasma electrolytic oxidation ceramic films formed on AZ31 magnesium alloy", The Chinese journal of Process Engineering, Vol.9(3), 592–597.*

6. *Yin Z, Tao S and Zhou X (2011), "Effect of the thickness on properties of Al_2O_3 coatings deposited by plasma spraying", Materials Characterization, Vol.62(1), 90–93.*

7. *Aruna S T, Balaji N, Jyothi Shedthi, William Grips V K (2012), "Effect of critical plasma spray parameters on the microstructure, microhardness and wear and corrosion resistance of plasma sprayed alumina coatings", Surface and Coatings Technology, Vol.208(15), 92-100.*
8. *Spencer K, Fabijanic D M, Zhang M X (2009), "The use of Al – Al_2O_3 cold spray coatings to improve the surface properties of magnesium alloys" Surface and Coatings Technology, Vol.204(3), 336–344.*
9. *Ozkan Sarikaya. (2005) "Effect of some parameters on microstructure and hardness of alumina coatings prepared by the air plasma spraying process", Surface and Coatings Technology, Vol.190(2-3), 388– 393.*
10. *Li J F, Liao H, Ding C X and Coddeta C (2005), "Optimizing the plasma spray process parameters of yttria stabilized zirconia coatings using a uniform design of experiments", Journal of Materials Processing Technology, Vol.160(1), 34–42.*
11. *Wang Y and Coyle T W (2008), "Optimization of Solution Precursor Plasma Spray Process by Statistical Design of Experiment", Journal of Thermal Spray Technology, Vol.17(5-6), 692-699.*
12. *Lin B T, Jean M D and Chou J H (2007), "Using response surface methodology with response transformation in optimizing plasma spraying coatings", International Journal of Advanced Manufacturing Technology, Vol.34 (3-4), 307–315.*
13. *Lin B T, Jean M D and Chou J H (2007), "Using response surface methodology for optimizing deposited partially stabilized zirconia in plasma spraying", Applied Surface Science, Vol.253(6), 3254–3262.*
14. *Ramachandran C S, Balasubramanian, V. and Ananthapadmanabhan, P.V. (2011) "On resultant properties of atmospheric plasma sprayed yttria stabilised zirconia coating deposits: designed experimental and characterisation analysis", Journal of Surface Engineering, Vol. 27(3), 217–229.*
15. *ASTM G 31-72., (2002), "Standard practice for laboratory immersion corrosion testing of metals", Pennsylvania: American Society for Testing of Materials.*
16. *Rajasekhar P, Ganesan G, and Senthilkumar C, (2014), "Modelling and optimization of tribological behavior of coconut and jute fibers with nano ZnO fillers on polymer matrix composites", Journal of Manufacturing Engineering, Vol. 9(4), 234-241.*
17. *Viswanathan G, Kannan, T T M, Abdulghani Khan M, Chandradass J and Giridharan S, "Optimization of mechanical properties of friction welding parameters of austenitic stainless steel (AISI 316) rods using design of experiments concept", Journal of Manufacturing Engineering, Vol. 10(2), 091-096.*
18. *Box G E P and Draper N R (1986), "Empirical Model-Building and Response Surfaces", John Wiley & Sons Inc, New York.*
19. *Bailey R A (2008), "Design of Comparative Experiments", Cambridge University Press, New York.*
20. *Khuri A I and Cornell J A (1996), "Response Surfaces; Design and Analysis", Marcel Dekker Ltd, New York.*
21. *Oktem H, Erzurumlu T and Kurtaran H (2005), "Application of response surface methodology in the optimization of cutting conditions for surface roughness", Journal of Materials Processing Technology, Vol.170(1-2), 11-16.*
22. *Kumaragurubaran B, Parthipa Saravana Kumar T, Senthil Kumar T and Chandrasekar M (2013), "Optimizing the Plasma Spray Process Parameters of Yttria Stabilized Coatings on Aluminum Alloy Using Response Surface Methodology", International Journal of Engineering and Advanced Technology, Vol. 2(5), 377–384.*
23. *Lakshminarayanan A K, Balasubramanian V, Varahamoorthy, R and Babu S (2008), "Predicting the dilution of plasma transferred arc hard facing of stellite on carbon steel using response surface methodology", Journal of Metals and Materials International, Vol.14 (6), 779-789.*
24. *Montgomery D C (2007), "Design and Analysis of Experiments", 5th ed., John Wiley & Sons, New York.*
25. *Shahi A S and Pandey S (2008), "Modelling of the effects of welding conditions on dilution of stainless steel claddings produced by gas metal arc welding procedures", Journal of Materials Processing Technology, Vol.196(1-3), 339-344.*
26. *Bertrand G, Bertrand P, Roy P, Rio C and Mevrel R (2008), "Low Conductivity Plasma Sprayed Thermal Barrier Coating Using Hollow PSZ Spheres: Correlation Between Thermo physical Properties and Microstructure", Surface and Coatings Technology, Vol.202(10), 1994-2001.*
27. *Guo H, Kuroda S and Murakami H (2006), "Microstructures and Properties of Plasma-Sprayed Segmented Thermal Barrier Coatings", Journal of American Ceramic Society, Vol.89(4), 1432-1439.*

